Chinese Chemical Letters 32 (2021) 3057–3060

Contents lists available at ScienceDirect

Chinese Chemical Letters

journal homepage: www.elsevier.com/locate/cclet

Communication

Monitoring intracellular pH fluctuation with an excited-state intramolecular proton transfer-based ratiometric fluorescent sensor

Bin Feng[a,b,c], Yingli Zhu[a,b,c], Jiaxin Wu[a,b,c], Xueyan Huang[a,b,c], Rong Song[a,b,c], Liu Huang[a,b,c], Xueping Feng[d], Wenbin Zeng[a,b,c,*]

[a] Xiangya School of Pharmaceutical Sciences, Central South University, Changsha 410013, China
[b] The Molecular Imaging Research Center, Central South University, Changsha 410013, China
[c] Hunan Key Laboratory of Diagnostic and Therapeutic Drug Research for Chronic Diseases, Central South University, Changsha 410013, China
[d] Xiangya Hospital, Central South University, Changsha 410013, China

ARTICLE INFO

Article history:
Received 3 February 2021
Received in revised form 25 March 2021
Accepted 26 March 2021
Available online 30 March 2021

Keywords:
Excited-state intramolecular proton transfer
Intracellular pH
Sulfonamide
Ratiometric sensor
Fluorescent imaging

ABSTRACT

Intracellular pH is a key parameter related to various biological and pathological processes. In this study, a ratiometric pH fluorescent sensor ABTT was developed harnessing the amino-type excited-state intramolecular proton transfer (ESIPT) process. Relying on whether the ESIPT proceeds normally or not, ABTT exhibited the yellow fluorescence in acidic media, or cyan fluorescence in basic condition. According to the variation, ABTT behaved as a promising sensor which possessed fast and reversible response to pH change without interference from the biological substances, and exported a steady ratiometric signal (I_{478}/I_{546}). Moreover, due to the ESIPT effect, large Stokes shift and high quantum yield were also exhibited in ABTT. Furthermore, ABTT was applied for monitoring the pH changes in living cells and visualizing the pH fluctuations under oxidative stress successfully. These results elucidated great potential of ABTT in understanding pH-dependent physiological and pathological processes.

Hydronium ion plays critical roles in many biological [1–3] and pathological processes [4–7]. Generally, the pH of normal tissue is carefully maintained at 7.2−7.4 [8], while abnormal changes in the pH gradient can be observed under pathological conditions, including cancer [9–11], sepsis [12], hyperkalemia [13], and chronic kidney disease [14]. For example, a lower pH (6.7∼7.1) is always found in tumor microenvironment. And these specific pH gradients in pathological tissues can be used as biomarkers for targeted therapy [15–19]. Furthermore, the imbalance of pH is also considered to be the cause of a variety of secondary diseases [4,20]. Acidosis, for instance, is an important component of the pathogenetic events that lead to ischemic brain damage [21]. Therefore, monitoring changes in intracellular pH is very important to understand these pH-dependent cellular behaviors and pathological processes. Although many methods for measuring intracellular pH such as microelectrodes [22], NMR [23], and absorbance spectroscopy [24] have been developed, but they suffer from several drawbacks such as low sensitivity, poor selectivity, complicated sampling process, and high cost [25]. By contrast, fluorescence spectroscopy exhibited the advantages of high sensitivity, ease-to-use and capability of visualizing the temporal and spatial changes of intracellular pH [26–28]. However, the traditional fluorescent sensors operating on the fluorescent intensity may be significantly affected by the environmental factors, including changes of optical path length, varied emission collection efficiencies, and altered excitation intensities. Ratiometric fluorescence probes or sensors work on the changes of two individual emission bands, by which they can efficiently self-calibrate to exclude the interference from the environment [29–31]. Nevertheless, the delicate difference in wavelength and serious crosstalk between emission bands still limits their effectiveness and resolution [32,33]. Therefore, it is still of significance to develop renewed ratiometric pH fluorescent sensors with optimized signals.

Herein, we developed a ratiometric fluorescent sensor 2-(2'-tosylamino-4'-chlorophenyl)benzothiazole (ABTT) allowing continuously monitoring pH in living cells. Upon appending with strong electron-withdrawing tosyl group, the amino-type excited-state intramolecular proton-transfer (ESIPT) process was favorable without apparent energy barriers. However, the process can be blocked partly or overwhelmingly upon deprotonation of

* Corresponding author at: Xiangya School of Pharmaceutical Sciences, Central South University, Changsha 410013, China.
E-mail address: wbzeng@csu.edu.cn (W. Zeng).

https://doi.org/10.1016/j.cclet.2021.03.074

sulfonamide moiety in basic condition. As a result, the sensor exhibits yellow fluorescence from tautomer form in acidic media while cyan fluorescence from deprotonation form in basic media (Scheme 1). Thanks to its unique working mechanism, ABTT inherited its innate excellent photostability and reversibility, as well as high quantum yield and large Stokes shift. More importantly, ABTT was further applied to imaging pH changes and monitoring pH fluctuations under oxidative stress in living cells.

ESIPT is a photophysical process occurring in fluorophores involving tautomerization upon excitation, in which a proton was transferred from the proton donor to acceptor [34,35]. Compared with the energetically favorable ESIPT involving phenolic hydroxyl group ($pK_a \approx 10$) [36], higher energy barrier exists in thermodynamic regimes in N—H type ESIPT due to the much weaker acidity of aromatic amino group ($pK_a \approx 30$) [37,38]. Interestingly, the acidity of the amine, together with the polarization of the N—H bond and the strength of the H-bond donor, can be modulated by the introduction of electron-withdrawing N-substituent at amino group, to give a substantial ESIPT driving force [39,40]. Further, the resultant tautomer fluorescence exhibited high sensitivity toward local surroundings, *e.g.*, the pH and polarization of solution [34]. Hence, 2-(2'-amino-4'-chlorophenyl)benzothiazole (ABT) was appended with a strong electron-withdrawing tosyl group to facilitate its ESIPT process, and endow it sensing capability toward local pH value. Sensor ABTT was facilely prepared by a four-step process and details of synthetic route were outlined in Scheme S1 (Supporting information) [41].

As a starting point, the solvent effect of ABT and ABTT was first investigated in various organic solvents. As shown in Fig. S2a (Supporting information), ABT exhibited only a sole fluorescent emission in various solvents with Stokes shift as little as ~90 nm, meaning the prohibition of ESIPT process. On the contrary, ESIPT underwent well in ABTT, and a dominant emission with large Stokes shift was observed in Hexane, THF, DCM and ethanol (Fig. 1a). While, the emission peak bule-shifted and broadened a lot in methanol, illustrating that the ESIPT process in ABTT was blocked partly. In MeCN, DMSO, and DMF, a further hypsochromic shift appeared and only an emission with little Stokes shift were observed, demonstrating that the substantial change of Stokes shift is not derived from the solvatochromism but the overwhelmingly blocked ESIPT process. These results demonstrate that ESIPT process proceeds without apparent energy barrier in ABTT upon tosyl substitution, and it can be tuned as well by the outer stimulation [42].

With this in mind, the absorbance and fluorescence spectra of ABTT at different pH was evaluated in aqueous solution (buffer/DMSO = 99.5:0.5 (v/v)). As shown in Fig. S1 (Supporting information), the maximal absorption peak red-shifted upon the media changing from acidic (pH 4) and basic (pH 9). In Fig. 1b, a sole emission peaked at 546 nm (fluorescent quantum yield (Φ) = 0.40, Table S2 in Supporting information) was observed in acidic media, while a new emission peaked at 478 nm (Φ = 0.58, Table S2) was observed in basic media. Importantly, owing to the ESIPT process, the sensor displayed large Stokes shift (186 nm/118 nm) in acidic

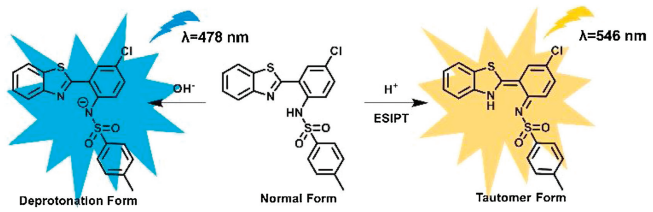

Scheme 1. The proposed sensing mechanism of ABTT toward acidic or basic media.

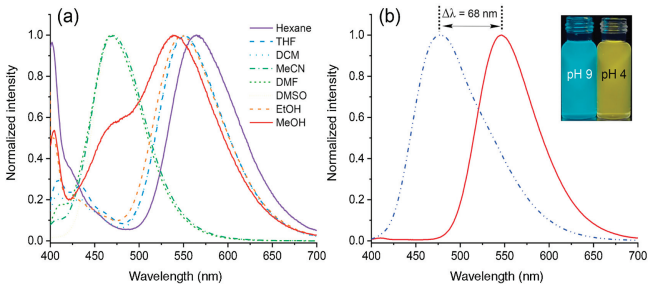

Fig. 1. Fluorescence emission spectra (λ_{ex} = 360 nm) of ABTT (10 μmol/L) in various organic solvents (a) and in acidic (pH 4, red solid line) and basic (pH 9, blue dash line) media (b). Inset: fluorescence images of ABTT in corresponding media under UV light (365 nm).

and basic media, respectively, which can distinctly reduce interference from the excitation and avoid self-reabsorption [34,43]. Compared with the significant change in ABTT, no noticeable spectral change was observed in ABT (Fig. S2b in Supporting information). Hence, the spectral shifts of ABTT can be attributed to the protonation (or deprotonation) of the sulfonamide moiety, thereby normally proceeding or blocking the process of ESIPT, as depicted in Scheme 1. Moreover, an apparent hypsochromic shift as large as 68 nm provides high resolution for monitoring pH in complex environment [32].

To rationalize the pH sensing mechanism, density functional theory (DFT) calculations for ABTT in different forms were conducted at B3LYP/6−31G(d, p) level (Gaussian 09 W) [39,44]. As shown in Fig. 2, the HOMO-LUMO gap of deprotonation form (4.08 eV) is smaller than that of normal form (4.14 eV), which is consistent to the red shift observed in the absorbance spectra (Fig. S1). Further, the obvious charge redistribution in the electronic density was observed in deprotonation form, supporting the red-shifted peak was ascribed to the deprotonated sensor in basic media. Moreover, the hypsochromic shift of fluorescence can also be attributed to the variation in the energy gap from 3.23 eV (tautomer form) to 4.08 eV (deprotonation form) [32]. To further support the existence of two forms, ^{1}H NMR titration experiment was carried out. As shown in Fig. S3 (Supporting information), a single peak corresponding to the sulfonamide proton at 12.13 ppm disappeared upon addition of TEA (1.0 equiv). The above results are consistent with our proposed mechanism that the apparent fluorescence emission depends on whether ESIPT in ABTT proceed well or not, and the large emission shift would happen once tautomer form is forbidden but deprotonation form is allowed, *e.g.*, the pH is changed.

Inspired by the proved feasibility of ABTT, our efforts were then turned into assessing the practical potential in ratiometric detection of pH values. A standard fluorescence pH titration of ABTT was performed in aqueous solution as shown in Fig. 3a. With the pH rising from 4.0 to 12.0, the emission of ABTT gradually hypsochromically shifted, behaving as that the intensity of the initial emission (I_{546}) dropped remarkably while the emerging

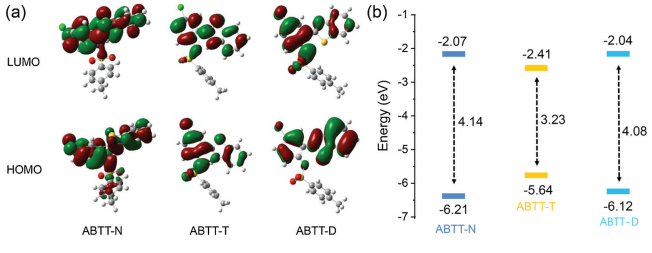

Fig. 2. Frontier molecular orbitals (a) and HOMO-LUMO energy levels (b) of ABTT-N (normal form), ABTT-T (tautomer form), and ABTT-D (deprotonation form).

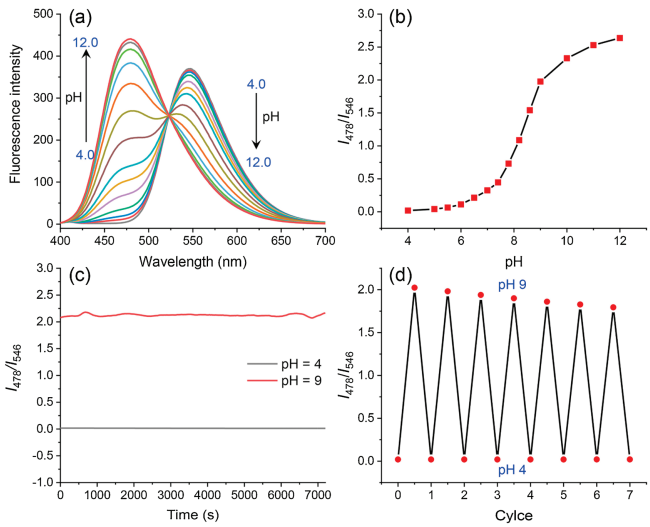

Fig. 3. (a) Fluorescence emission spectra of ABTT (10 μmol/L) in aqueous solution (pH 4.0~12.0). (b) Plots of fluorescence intensity ratio (I_{478}/I_{546}) of ABTT (10 μmol/L) *versus* pH. (c) Change in fluorescence ratio (I_{478}/I_{546}) of ABTT (10 μmol/L) at pH 4.0, and 9.0, respectively. (b) Reversible fluorescence changes of ABTT (10 μmol/L) between pH 4.0 and pH 9.0. λ_{ex} = 360 nm.

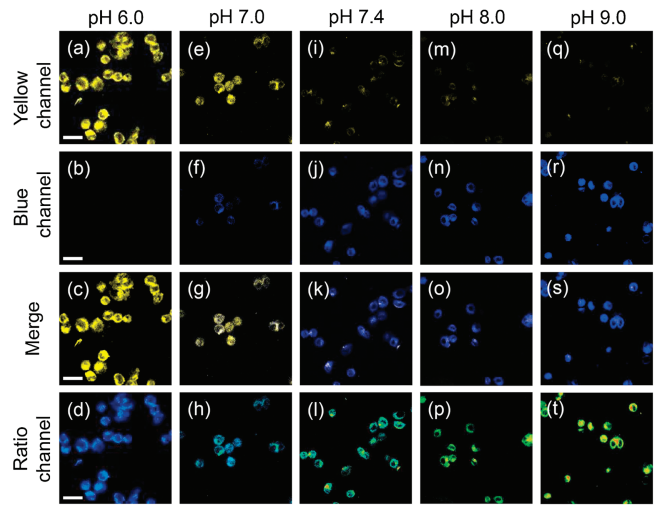

Fig. 4. Fluorescent images of ABTT (10 μmol/L) in HepG2 cells clamped at pH 6.0 (a-d), 7.0 (e-h), 7.4 (i-l), 8.0 (m-p) and 9.0 (q-t), respectively. The signals were collected at 450-530 nm (yellow channel, 1st row) and 570-610 nm (blue channel, 2nd row) upon excitation at 405 nm. The 3rd row exhibited the corresponding merge images and the 4th (ratio channel) were obtained by ImageJ software. Scale bar: 50 μm.

emission (I_{478}) raised a lot. The hypsochromical shift appeared as the distinct fluorescence color changing from yellow to cyan, which can be easily distinguished by bared eye (Fig. S4 in Supporting information). An isoemissive point can be seen at 523 nm, so the detailed fluorescence ratio I_{478}/I_{546} can be measured versus pH. As illustrated in Fig. 3b, it was easy to determine the pH value based on the fluorescence ratio, making it applicable for preliminary and wide-range pH fluctuation detection.

High photostability is a determinant requirement for the practical applications in long-term pH monitoring [45]. The photostability of ABTT was evaluated under the excitation of a 150 W xenon lamp, and intensity at 546 and 478 nm in acidic and basic media were collected respectively for 2.5 h. Obviously, the fluorescent intensities and the corresponding ratiometric signals were relatively stable during the scanning period (Fig. S5 in Supporting information and Fig. 3c), indicating that ABTT was highly sensitive to pH changes but stable to light, media and air. Moreover, ABTT displayed a good reversibility when the media pH circularly changing between 4.0 and 9.0 forth and back, and still retained high sensitivity toward pH change even after seven recycles (Fig. 3d). Then determining interference from other biological molecules was taken account, as shown in Fig. S6 (Supporting information), no obvious variation in the fluorescent intensities was triggered by the relevant species. From these results, it can be concluded that ABTT possesses a fast and reversible response to pH changes without interference from the biological substances, and exports a stable ratiometric signal, all are beneficial for the real-time and long-term pH monitoring in complex matrices.

Having demonstrated *in vitro* ABTT was favorable for the biological pH detection, its capacity for monitoring the intracellular pH changes was accessed. First, the cytotoxicity of ABTT on HepG2 cells were evaluated using CCK8 assay (Fig. S7 in Supporting information). Apparently, ABTT at concentration as large as 20 μmol/L have not exhibited distinct toxicity to the living cells (survival rate > 90%), indicating its low cytotoxicity and excellent biocompatibility. In addition, HepG2 cells incubated with ABTT (10 μmol/L) for 20 min exhibited intensive fluorescent signals in the blue channel and weak signals in the yellow channel (Fig. S8 in Supporting information), confirming the excellent cell membrane permeability of ABTT. Encouraged by the above results, the applicability of ABTT to detect intracellular pH value was taken account. To calibrate the intracellular pH, HepG2 cells were treated with H^+/K^+ ionophore nigericin (10 μmol/L) to homogenizing the pH with different value [32,33]. As displayed in Fig. 4, the living cells pre-stained with ABTT at pH 6.0 exhibited strong fluorescence in yellow channel and almost no fluorescence in the blue channel. However, the fluorescent intensity in yellow channel declined gradually whereas that in blue channel grew higher when the intracellular pH value elevated from 6 to 9, allowing ratiometric monitoring the pH changes in living cells. Importantly, remarkable pseudocolor variations were observed between pH 7.0 and 8.0, demonstrating the high potential of ABTT in monitoring intracellular pH fluctuations.

As one of the central chemical reaction, intracellular redox has been reported to involve in pH homeostasis [46]. Considering this, the practical capability of ABTT in monitoring slight pH fluctuation in living cells was assessed under the stimulation of various redox substances. In the above anti-interference experiments, the normal redox substances have been validated without interference toward ABTT. First, H_2O_2 and NaClO were applied to ABTT-prestained HepG2 cells and then imaged as shown in Fig. 5. Compared with untreated cells, a significant increase of fluorescence in yellow channel and slight fall in blue channel was induced by H_2O_2, indicating the acidification of intracellular cytosol. This may be ascribed to the H_2O_2-produced hydroxyl radicals which further generates some acidic substances to cause acidification of cells [47]. On the contrary, low intracellular pH was not induced by ClO^- due to its incapability of elevating the level of intracellular pH, which was in line with the previous reports [32,33]. In addition, the reduction of GSH level is reported with capacity to affect the function of the Na^+/H^+ antiporter, herein, *N*-ethylmaleimide (NEM, a GSH depletor) and *N*-acetylcysteine (NAC, a GSH precursor) were treated with HepG2 cells, respectively, to regulate the intracellular GSH level [32]. As expected, the treatment of NEM triggered the decline of intracellular pH, by contrast, no obvious pH change was reflected in NAC-treated cells, which can be explained by non-influence of elevated GSH level on intracellular acidic substances [32,33]. More apparently, the pH fluctuations induced by oxidative stress can be distinguished facilely according to the pseudocolor images. These results suggest

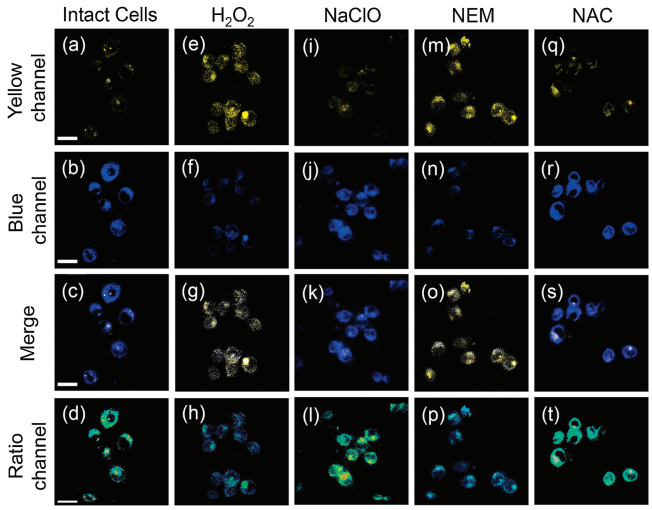

Fig. 5. Fluorescent images of ABTT (10 μmol/L) in intact HepG2 cells (a-d) and cells treated with 100 μmol/L H_2O_2 (e-h), 100 μmol/L NaClO (i-l), 1.0 mmol/L NEM (m-p), and 1.0 mmol/L NAC (q-t). The signals were collected at 450–530 nm (yellow channel, 1st row) and 570–610 nm (blue channel, 2nd row) upon excitation at 405 nm. The 3rd row exhibited the corresponding merge images, and the 4th (ratio channel) were obtained by ImageJ software. Scale bar: 30 μm.

the good capability of sensor ABTT to explore the relationship between intracellular pH fluctuations and oxidative stress, and it will be a promising tool for analyzing various pH-dependent biological and pathological processes as well.

In summary, a novel ratiometric pH fluorescent sensor ABTT was synthesized *via* a condensation of 2-(2'-amino-4'-chlorophenyl)benzothiazole with tosyl group. Upon appending of tosyl group, amino-type ESIPT process was thermodynamically allowed, endowing ABTT a long-wavelength emission with large Stokes shift in acidic media. On the contrary, the deprotonation in sulfonamide moiety blocked the ESIPT process partly or overwhelmingly in basic condition, giving the hypsochromically shifted emission. The significant color change from yellow to cyan allowed less spectral overlap and higher spatial resolution for pH detection. Moreover, the excellent photostability and reversibility, high quantum yield, and favorable anti-interference allowed its application in imaging pH changes in living cells and monitoring pH fluctuations under oxidative stress. These results elucidates that the sensor may potentially be used in understanding pH-dependent biological and pathological processes.

Declaration of competing interest

The authors report no declarations of interest.

Acknowledgments

We are grateful for the financial supports from National Natural Science Foundation of China (Nos. 81971678 and 81671756) and the Innovation Fund for Postgraduate Students of Central South University (No. 2019zzts1019).

Appendix A. Supplementary data

Supplementary material related to this article can be found, in the online version, at doi:https://doi.org/10.1016/j.cclet.2021.03.074.

References

[1] K.O. Alfarouk, S.B.M. Ahmed, R.L. Elliott, et al., Metabolites 10 (2020) 285–301.
[2] K.A. White, B.K. Grillo-Hill, M. Esquivel, et al., J. Cell Biol. 217 (2018) 3965–3976.
[3] L. Zhou, Z. Jin, X. Fan, et al., Chin. Chem. Lett. 29 (2018) 1500–1502.
[4] M.A. Ramirez, A.R. Beltran, J.E. Araya, et al., Curr. Vasc. Pharmacol. 17 (2019) 440–446.
[5] K.A. White, K. Kisor, D.L. Barber, Cancer Metast. Rev. 38 (2019) 17–24.
[6] L.A. Calo, P.A. Davis, Int. J. Mol. Sci. 21 (2020) 5660–5669.
[7] Y. Yan, X. Zhang, X. Zhang, et al., Chin. Chem. Lett. 31 (2020) 1091–1094.
[8] B. Shi, Y. Gao, C. Liu, et al., Dye. Pigment. 136 (2017) 522–528.
[9] J. Chiche, M.C. Brahimi-Horn, J. Pouyssegur, J. Cell. Mol. Med. 14 (2010) 771–794.
[10] C. Corbet, O. Feron, Nat. Rev. Cancer 17 (2017) 577–593.
[11] S.R. Pillai, M. Damaghi, Y. Marunaka, et al., Cancer Metast. Rev. 38 (2019) 205–222.
[12] B. Suetrong, K.R. Walley, Chest 149 (2016) 252–261.
[13] A.N. Harris, P.R. Grimm, H.W. Lee, et al., J. Am. Soc. Nephrol. 29 (2018) 1411–1425.
[14] J. Harambat, K. Kunzmann, K. Azukaitis, et al., Kidney Int. 92 (2017) 1507–1514.
[15] B.E.F. de Avila, D.E. Ramirez-Herrera, S. Campuzano, et al., ACS Nano 11 (2017) 5367–5374.
[16] X.B. Zhao, Z.H. Wei, Z.P. Zhao, et al., ACS Appl. Mater. Inter. 10 (2018) 6608–6617.
[17] J.R. Hou, D. Jin, B. Chen, et al., Chin. Chem. Lett. 28 (2017) 1681–1687.
[18] C.T.H. Nguyen, R.I. Webb, L.K. Lamber, et al., ACS Appl. Mater. Inter. 9 (2017) 9470–9483.
[19] Z. Shi, Q. Li, L. Mei, Chin. Chem. Lett. 31 (2020) 1345–1356.
[20] W.E. Mitch, R. Medina, S. Grieber, et al., J. Clin. Invest. 93 (1994) 2127–2133.
[21] B.K. Siesjo, Neurochem. Pathol. 9 (1988) 31–88.
[22] S.R. Ng, D. O'Hare, Analyst 140 (2015) 4224–4231.
[23] S. Adler, E. Shoubridge, G.K. Radda, Am. J. Physiol. 247 (1984) 188–196.
[24] T. Matsumoto, T. Tomita, Jpn. J. Physiol. 43 (1993) 103–109.
[25] J.Y. Han, K. Burgess, Chem. Rev. 110 (2010) 2709–2728.
[26] H. Zhang, P. Xu, X. Zhang, et al., Chin. Chem. Lett. 31 (2020) 1083–1086.
[27] J.T. Hou, W.X. Ren, K. Li, et al., Chem. Soc. Rev. 46 (2017) 2076–2090.
[28] X.L. Huang, J.B. Song, B.C. Yung, et al., Chem. Soc. Rev. 47 (2018) 2873–2920.
[29] W. Shi, X.H. Li, H.M. Ma, Angew. Chem. Int. Ed. 51 (2012) 6432–6435.
[30] Y. He, Z. Li, Q. Jia, et al., Chin. Chem. Lett. 28 (2017) 1969–1974.
[31] H. Li, H. Dong, M. Yu, et al., Anal. Chem. 89 (2017) 8863–8869.
[32] L.X. Cao, X.Y. Li, S.Q. Wang, et al., Chem. Comm. 50 (2014) 8787–8790.
[33] Y.H. Li, Y.J. Wang, S. Yang, et al., Anal. Chem. 87 (2015) 2495–2503.
[34] A.C. Sedgwick, L.L. Wu, H.H. Han, et al., Chem. Soc. Rev. 47 (2018) 8842–8880.
[35] J.E. Kwon, S.Y. Park, Adv. Mater. 23 (2011) 3615–3642.
[36] A.P. Demchenko, K.C. Tang, P.T. Chou, Chem. Soc. Rev. 42 (2013) 1379–1408.
[37] T.P. Smith, K.A. Zaklika, K. Thakur, P.F. Barbara, J. Am. Chem. Soc. 113 (1991) 4035–4036.
[38] C.L. Chen, Y.T. Chen, A.P. Demchenko, P.T. Chou, Nat. Rev. Chem. 2 (2018) 131–143.
[39] H.W. Tseng, J.Q. Liu, Y.A. Chen, et al., J. Phys. Chem. Lett. 6 (2015) 1477–1486.
[40] C.L. Chen, H.W. Tseng, Y.A. Chen, et al., J. Phys. Chem. A 120 (2016) 1020–1028.
[41] Y. Liu, B. Feng, X.Z. Cao, et al., Analyst 144 (2019) 5136–5142.
[42] W.H. Song, B.L. Dong, Y.R. Lu, W. Lin, Tetrahedron Lett. 60 (2019) 1696–1701.
[43] L.W. He, B.L. Dong, Y. Liu, W. Lin, Chem. Soc. Rev. 45 (2016) 6449–6461.
[44] B. Feng, Y. Liu, S. Huang, et al., Sens. Actuators B: Chem. 325 (2020) 128786–128796.
[45] H.Y. Si, M.K. Cho, J.S. Kang, et al., Anal. Chem. 90 (2018) 8058–8064.